

Feed-Rate-Limited Aerosol-Assisted Chemical Vapor Deposition of $\text{Cd}_x\text{Zn}_{1-x}\text{S}$ and ZnS:Mn with Composition Control

M. Nyman,[†] K. Jenkins,[†] M. J. Hampden-Smith,^{*,†} T. T. Kodas,[‡] and E. N. Duesler[†]

Departments of Chemistry and Chemical Engineering and Center for Micro-Engineered Materials, University of New Mexico, Albuquerque, New Mexico 87131

A. L. Rheingold and M. L. Liable-Sands

Department of Chemistry, University of Delaware, Newark, Delaware 19716

Received October 15, 1997. Revised Manuscript Received January 8, 1998

Doped group 12 metal sulfides are important materials in the phosphor display industry. Control over the host lattice phase, composition, and dopant concentration is crucial for controlling the luminescence characteristics of these materials. Ternary thin films of $\text{Cd}_x\text{Zn}_{1-x}\text{S}$ and ZnS:Mn were deposited by aerosol-assisted chemical vapor deposition (AACVD) using liquid delivery of toluene solutions of new single-source Zn–S and Cd–S precursors $\text{M}(\text{SOCC}(\text{CH}_3)_3)_2\text{TMEDA}$ ($\text{M} = \text{Cd}, \text{Zn}$; $\text{TMEDA} = N,N,N,N$ -tetramethylethylenediamine) and $\text{Mn}_2(\text{CO})_{10}$ as a source of Mn. Control over film composition, wherein the precursor solution and film stoichiometries were identical, was achieved by using feed-rate-limited deposition conditions. Films with compositions $\text{Cd}_{0.75}\text{Zn}_{0.25}\text{S}$, $\text{Cd}_{0.50}\text{Zn}_{0.50}\text{S}$, and $\text{Cd}_{0.25}\text{Zn}_{0.75}\text{S}$ were deposited at 225 °C from 10 mmol solutions with the same Cd:Zn precursor mole ratios, respectively. A series of control experiments in which the precursor feed rate was varied confirmed the presence of feed-rate-limited film growth. Films of ZnS:Mn with 1–8 at. % Mn dopant levels were also deposited from solutions with the same Zn:Mn precursor mole ratios, respectively, using feed-rate-limited deposition strategies.

Introduction

The group 12 metal sulfides CdS, ZnS, and $\text{Cd}_x\text{Zn}_{1-x}\text{S}$ are technologically important materials which have been used in the form of thin films for a variety of applications including optical coatings, solid-state solar cell windows, electrooptic modulators, photoconductors, field effect transistors, sensors, and transducers.^{1,2} More recently, there has been great interest in doped group 12 metal sulfide materials for display technologies as cathodoluminescent (i.e., ZnS:Cu , ZnS:Ag , $\text{Cd}_x\text{Zn}_{1-x}\text{S:S:Cu}$, or $\text{Cd}_x\text{Zn}_{1-x}\text{S:Ag}$) or electroluminescent (i.e., ZnS:Mn)^{3,4} materials. The luminescence behavior of doped group 12 metal sulfides is greatly influenced by film characteristics including crystallinity, density, purity, phase, dopant levels, and, in the case of $\text{Cd}_x\text{Zn}_{1-x}\text{S}$, composition. For example, the emission color of $\text{Cd}_x\text{Zn}_{1-x}\text{S:Ag}$ varies approximately linearly with composition (x) from 400 nm (Zn rich) to 700 nm (Cd rich).³ Control over dopant levels is also important for

obtaining luminescent materials with optimum properties. For example, ZnS:Mn luminesces most efficiently with a dopant level of 1% Mn substitution for Zn.^{4,5} Metal sulfide films have been deposited by a variety of different methods including physical and chemical vapor deposition (PVD and CVD).

Previous work by Xu et al.¹⁴ on aerosol-assisted (AA) CVD of binary films from two precursors demonstrated that the feed-rate-limited film-growth regime facilitates compositional control so that the film has a composition identical to the precursor solution. In this operating regime, all of the reactant molecules reaching the

[†] Department of Chemistry.

[‡] Department of Chemical Engineering.

(1) Hovel, H. J. *Semiconductors and Semimetals*; Academic: New York, 1975; Vol. 11.

(2) Nicolau, Y. F.; Dupuy, M.; Brunel, M. *J. Electrochem. Soc.* **1990**, *137*, 2915–2924.

(3) Braithwaite, N.; Weaver, G. *Electronic Materials*; Butterworth: London, 1990.

(4) Rack, P. D.; Naman, A.; Holloway, P. H.; Sun, S.-S.; Tuenge, R. T. *MRS Bull.* **1996**, *21*, 49–58.

(5) Miyata, T.; Minami, T.; Takata, S. *J. Cryst. Growth* **1992**, *117*, 1021–1025.

(6) Cotton, F. A.; Wilkinson, G. *Advanced Inorganic Chemistry*, 5th ed.; John Wiley and Sons: New York, 1988.

(7) Nyman, M.; Hampden-Smith, M. J.; Duesler, E. N. *Adv. Mater. CVD* **1996**, *5*, 171–174.

(8) Frigo, D. M.; Khan, O. F. Z.; O'Brien, P. *J. Cryst. Growth* **1989**, *96*, 989.

(9) Migita, M.; Kanehisa, O.; Shiiki, M.; Yamamoto, H. *J. Cryst. Growth* **1988**, *93*, 686–691.

(10) Hirabayashi, K.; Kozawaguchi, H. *Jpn. J. Appl. Phys.* **1986**, *25*, 711–713.

(11) Yasuda, T.; Hara, K.; Mizuta, M.; Kukimoto, H. *J. Cryst. Growth* **1989**, *96*, 979–981.

(12) Minami, T.; Miyata, T.; Kitamura, K.; Nanto, H.; Takata, S. *Jpn. J. Appl. Phys.* **1988**, *27*, L876–L879.

(13) McLaughlin, M.; Sakeek, H. F.; Maguire, P.; Graham, W. G.; Molloy, J.; Morrow, T.; Laverty, S.; Anderson, J. *Appl. Phys. Lett.* **1993**, *63*, 1865–1867.

(14) Xu, C.; Hampden-Smith, M. J.; Kodas, T. T. *Chem. Mater.* **1995**, *7*, 1539–1546.

surface react rapidly. As a result, the composition of the film has the same composition as the feed rate to the surface. These conditions may be facilitated by a relatively high preheating temperature, high substrate temperature, low carrier gas flow rate, and dilute precursor solutions. Alternative growth rate regimes include transport-limited, evaporation-rate-limited, and surface-reaction-limited growth.¹⁵ Transport-limited growth is limited by the rate of diffusion of the precursor to the substrate. Generally, we do not encounter precursor diffusion-limited growth based upon our deposition rates, which are relatively low. For evaporation-rate-limited deposition, the rate of evaporation of the precursor limits the concentration of the precursor in the vapor phase, and this situation is frequently encountered in AACVD. Finally, in the surface-reaction-limited growth regime, the rate of the surface reaction is the rate-limiting step of film growth. Film growth rates vary logarithmically with deposition or evaporation temperature within these thermally activated growth regimes (evaporation-limited and surface-reaction-limited), whereas film-growth rate is independent of deposition and evaporation temperature within the feed-rate-limited growth regime.

One final consideration for feed-rate-limited AACVD is that the precursors should not undergo gas-phase decomposition at the substrate temperatures (i.e., 250–300 °C) required for feed-rate-limited growth. Evidence for gas-phase decomposition was observed during AACVD of $M(\text{SOCC}(\text{CH}_3)_2)\text{TMEDA}$ ($M = \text{Cd}, \text{Zn}$) precursors.⁷ For this reason, the thiopivalate analogues $M(\text{SOCC}(\text{CH}_3)_2)\text{TMEDA}$ ($M = \text{Cd}, \text{Zn}$) were used as the precursors for these studies, since solution-phase studies of group 12 metal thiocarboxylates have shown that the thiopivalate compounds are more thermally stable toward thiocarboxylic anhydride elimination than the thioacetate compounds.¹⁶

Furthermore, we chose identical ligands for both Zn and Cd derivatives to avoid problems, such as precipitation, associated with ligand exchange, and to achieve similar or matched reactivities. "Matched reactivity" through identical precursor ligands is useful for achieving CVD of materials with compositional control from multiple precursor sources. For example, we recently reported that AACVD of $\text{Cd}_x\text{Zn}_{1-x}\text{S}$ from precursor solutions of mixtures of $\text{Cd}(\text{SOCC}(\text{CH}_3)_2)\text{TMEDA}$ and $\text{Zn}(\text{SOCC}(\text{CH}_3)_2)\text{TMEDA}$ produced films that were (1) depleted in Cd relative to the precursor solution, due to gas-phase reactions of the more reactive cadmium precursor at higher deposition temperatures (>175 °C), and (2) depleted in zinc relative to the precursor solution at lower temperatures (<175 °C) due to the higher surface reactivity of the cadmium precursor.⁷ Frigo et al. reported CVD of $\text{Cd}_x\text{Zn}_{1-x}\text{S}$ from zinc and cadmium dialkyldithiocarbamates where the resulting films were depleted in zinc relative to the precursor concentration in the reactor also due to the higher reactivity of the cadmium precursor.⁸ In both examples, composition control was not achieved from precursors with matching ligands, and therefore other factors such as CVD deposition conditions have to be examined.

Turning to a consideration of control over dopant concentration, unlike Zn and Cd, Zn and Mn do not have similar reactivity characteristics,⁶ so ligands that give similar reactivities for the zinc and manganese precursors to $\text{ZnS}:\text{Mn}$ must be determined through thermal decomposition or CVD experiments. The importance of matched reactivity of precursors for CVD of $\text{ZnS}:\text{Mn}$ was demonstrated in a study by Migita et al.⁹ The CVD of ZnEt_2 , H_2S , and either $\text{Mn}(\text{Cp})_2$ or $\text{Mn}(\text{Cp}-\text{Me})_2$ at 300 °C gave $\text{ZnS}:\text{Mn}$. However, CVD of ZnEt_2 , H_2S , and $\text{Mn}(\text{CO})_3(\text{Cp}-\text{Me})$ gave ZnS films without Mn dopant, due to the much lower reactivity of the Mn precursor at 300 °C. Additionally, Migita's study and other studies^{10,11} of CVD of $\text{ZnS}:\text{Mn}$ from separate Zn and Mn precursors did not report the ability to control dopant levels. Finally, alternative syntheses of $\text{ZnS}:\text{Mn}$ films such as thermal diffusion of the Mn into a ZnS film^{5,12} or ablation of a $\text{ZnS}:\text{Mn}$ target¹³ have not provided good control over dopant levels.

In this study, synthesis and characterization of the species $M(\text{SOCC}(\text{CH}_3)_2)\text{TMEDA}$ ($M = \text{Cd}, \text{Zn}$) as precursors to the corresponding metal sulfide films is reported. The growth kinetics of $\text{Cd}_x\text{Zn}_{1-x}\text{S}$ deposited by AACVD of $M(\text{SOCC}(\text{CH}_3)_2)\text{TMEDA}$ ($M = \text{Cd}, \text{Zn}$) is examined to determine the conditions of feed-rate-limited growth under which compositional control may be achieved. Preliminary studies on deposition of $\text{ZnS}:\text{Mn}$ (at. % Mn = 1–8) by AACVD of $\text{Zn}(\text{SOCC}(\text{CH}_3)_2)\text{TMEDA}$ and $\text{Mn}_2(\text{CO})_{10}$ with control over dopant levels is also reported.

Experimental Section

Synthesis and Characterization of $\text{Cd}(\text{SOCC}(\text{CH}_3)_2)\text{TMEDA}$ (1) and $\text{Zn}(\text{SOCC}(\text{CH}_3)_2)\text{TMEDA}$ (2). *General Techniques and Instrumentation.* Toluene was dried over sodium, distilled, and stored under dinitrogen over 3 Å predried molecular sieves. Thiopivalic acid was synthesized by the reaction of H_2S and trimethylacetyl chloride in pyridine and distilled twice to remove orange-colored impurities.¹⁷ *N,N,N,N*-Tetramethylethylenediamine (TMEDA) was purchased from Aldrich, stirred over sodium, and distilled prior to use. Synthesis of **2** was carried out using standard drybox and Schlenk line techniques. All other reagents were purchased and used without further preparation.

The crystalline species **1** and **2** were characterized by carbon, hydrogen, and nitrogen elemental analyses, ^1H , $^{13}\text{C}\{^1\text{H}\}$, and ^{113}Cd (where appropriate) nuclear magnetic resonance (NMR) spectroscopy, thermogravimetric analysis (TGA), FTIR, and single-crystal X-ray diffraction for structural analysis. The NMR data were recorded on a Bruker AC-250. The ^{113}Cd NMR spectra were recorded using an inverse-gated decoupling pulse program to accommodate for the negative NOE of the ^{113}Cd nucleus ($\gamma = -0.6217$). Typical parameters for ^{113}Cd spectra include a sweep width of 55 555 Hz, 10 s relaxation delay, and 100–5000 scans, and peaks were referenced externally to an aqueous solution of $\text{Cd}(\text{SO}_4)$ (5 ppm). Carbon, hydrogen, and nitrogen elemental analyses were carried out on a Perkin-Elmer 2400 elemental analyzer. The error was 0.3% for wt % carbon, 0.1% for wt % hydrogen, and 0.4% for wt % nitrogen. Thermogravimetric analyses (TGA) were performed on a Perkin-Elmer TGA 7700 thermogravimetric analyzer. Typical TGA experiments were carried out by heating the sample from 30 to 600 °C at a rate of 10 °C/min under a dinitrogen purge. The FTIR spectra were recorded on a Perkin-Elmer 1620 instrument as 1–5 wt % dispersion in KBr. Single-crystal X-ray diffraction data for **1** was collected on a Siemens R3m/V diffractometer in the Department of Chemistry at the University of New Mexico. Single-crystal X-ray diffraction data for **2** were collected on a Siemens P4m/v diffractometer at the University of Delaware.

(15) Kodas, T. T.; Hampden-Smith, M. J. *The Chemistry of Metal CVD*; VCH: Weinheim, 1994.

(16) Nyman, M. D.; Hampden-Smith, M. J.; Duesler, E. N. *Inorg. Chem.*, **1997**, in press.

Cd(SOCC(CH₃)₃)₂TMEDA (1). Cadmium carbonate (1.0 g, 5.8 mmol), TMEDA (0.673 g, 5.80 mmol), and toluene (20 mL) were combined in a round-bottom flask. Thiopivalic acid (1.5 mL, 12 mmol) was added to the mixture via pipet while stirring rapidly. The reaction took place immediately, noted by the disappearance of the solid cadmium carbonate and CO₂ bubble formation, and the resulting clear solution took on a yellow color. The toluene and volatile byproducts of the reaction water were removed under reduced pressure, and a glassy, creamy solid remained. The solid was redissolved in pentane and crystallized as long colorless needles at 3 °C, yield 2.2 g (82% yield based on cadmium carbonate).

Analytical data: elemental analysis calcd; 41.5% C, 7.4% H, 6.1% N. Found: 41.3% C, 7.3% H, 6.0% N. Thermogravimetric analysis: decomposition was completed around 200–250 °C in a single step. Inorganic residue was CdS by XRD; % (FW (1)/FW (CdS)) = 31% (found 30%). Infrared data: C=O 1578 cm⁻¹; C–S 967 cm⁻¹, 929 cm⁻¹. NMR data (C₆D₆, ppm): ¹H NMR 1.39 [18H, SOCC(CH₃)₃], 1.82 [4H, C₂H₄–TMEDA], ³J(¹¹³Cd–¹¹¹Cd) = 4.3 Hz (area of satellites = 25% of major peak), 2.05 [12H, CH₃–TMEDA], ³J(¹¹³Cd–¹¹¹Cd) = 4.5 Hz (area of satellites = 25% of major peak). ¹³C{¹H} NMR 29.5 [SOCC(CH₃)₃], 46.2 [CH₃–TMEDA], 47.3 [SOCC(CH₃)₃], 56.7 [C₂H₄–TMEDA]. ¹¹³Cd NMR 335.6.

Zn(SOCC(CH₃)₃)₂TMEDA (2). Diethylzinc (1.0 g, 8.1 mmol), TMEDA (0.94 g, 8.1 mmol), and toluene (20 mL) were combined in a round-bottom flask in a drybox. The flask was removed from the drybox, and thiopivalic acid (1.9 g, 16 mmol) was added to the mixture by pipet, while stirring rapidly. The reaction took place immediately, noted by formation of bubbles (ethane) and a white precipitate. The mixture was warmed to room temperature, and after an hour the toluene and volatile byproducts of the reaction ethane were removed under reduced pressure, and a glassy, creamy solid remain. The solid was redissolved in pentane and crystallized as colorless prisms, yield 3.4 g (100% yield based on diethylzinc).

Analytical data: elemental analysis calcd: 46.2% C, 8.2% H, 6.7% N. Found: 46.3% C, 8.4% H, 6.6% N. Thermogravimetric analysis: decomposition was completed around 200–250 °C in a single step. Inorganic residue was ZnS by XRD; % (FW (2)/FW (ZnS)) = 23% (found 22%). Infrared data: C=O 1612 cm⁻¹; C–S 962 cm⁻¹. ¹H NMR 1.39 [18H, SOCC(CH₃)₃], 1.99 [4H, C₂H₄–TMEDA], 2.15 [12H, CH₃–TMEDA]. ¹³C{¹H} NMR 29.15 [SOCC(CH₃)₃], 46.5 [CH₃–TMEDA], 48.0 [SOCC(CH₃)₃], 56.7 [C₂H₄–TMEDA].

Structural Characterization of Cd(SOCC(CH₃)₃)₂TMEDA (1) and Zn(SOCC(CH₃)₃)₂TMEDA (2). Single-crystal X-ray diffraction data for **1** were collected on a Siemens R3m/V diffractometer in the Department of Chemistry at the University of New Mexico. Single-crystal X-ray diffraction data for **2** was collected on a Siemens P4m/v diffractometer at the University of Delaware. Of 24 581 data collected for **1**, 11 793 were independent and 7610 were observed. The structure was solved by Patterson methods. All atoms were refined anisotropically, and all hydrogen atoms positions were allowed to vary. Of 4521 data collected for **2**, 4292 were independent and 2881 were observed. The structure was solved by direct methods. All non-hydrogen atoms were refined anisotropically, all hydrogen atoms positions were allowed to vary, the Flack parameter refined to –0.02(2) indicating that the correct absolute hand of the structure was determined. The crystallographic data and experimental details for **1** and **2** are summarized in Table 1. Relevant bond lengths and bond angles for **1** and **2** are listed in Tables 2 and 3, respectively.

Crystal Data for Cd(SOCC(CH₃)₃)₂TMEDA (1). CdS₂·O₂C₁₆H₃₄N₂, monoclinic, *P*2₁/*C*, *a* = 21.832 (3) Å, *b* = 22.452 (2) Å, *c* = 14.821 (1) Å; β = 102.85(1)°; *V* = 7082.8 (2) Å³; *Z* = 12; *D*_c = 1.302 g/cm³; μ(Mo Kα) = 1.110 mm⁻¹; *T* = 20 °C, Siemens R3m/v, Mo Kα. Of 24 581 data, (2 ≤ 2θ ≤ 49), 11 793 were independent and 7610 were observed [2σ(*F*_o)]. The structure was solved by Patterson methods. Refinement: all atoms were refined anisotropically, and all hydrogen atoms positions were allowed to vary, *R*(*F*) = 4.10%, *R*(*W*) = 3.77%, *GOF* = 1.08, *N*_o/*N*_v = 12.5, Δ(*r*) = 0.51 e Å⁻³, Δσ(max) = 0.067.

Table 1. Summary of Crystallographic Data for 1 and 2

	Cd(SOCC(CH ₃) ₃) ₂ TMEDA (1)	Zn(SOCC(CH ₃) ₃) ₂ TMEDA (2)
formula	C ₁₆ H ₃₄ CdN ₂ S ₂ O ₂	C ₁₆ H ₃₃ N ₂ S ₂ O ₂ Zn
FW	561.1	415.9
color	colorless	colorless plate
habit	transparent prism	
<i>a</i> , Å	21.832(3)	10.0859(9)
<i>b</i> , Å	22.452(2)	10.867(1)
<i>c</i> , Å	14.821(1)	19.986(3)
α, deg		
β, deg	102.85(1)	
γ, deg		
crystal system	monoclinic	orthorhombic
space group	<i>P</i> 2 ₁ / <i>C</i>	<i>P</i> 2 ₁ 2 ₁ 2 ₁
ρ (calc), g/cm ³	1.302	1.261
<i>T</i> /K	293	233
λ/Å	0.71073	0.71073
<i>Z</i>	12	4
crystal size/mm	0.30 × 0.57 × 0.69	0.40 × 0.40 × 0.12
<i>V</i> , Å ³	7082.8(11)	2190.6(4)
indep reflns	11,793	4292
obsvd reflns	7610	229
abs coeff, mm ⁻¹	1.110	1.321
<i>R</i> (<i>F</i>) % ^a	6.98	7.03
<i>R</i> _w (<i>F</i>) % ^b	5.10	9.58
<i>GOF</i>	1.08	0.978

$$^a R = \sum \Delta F / \sum F_o, \quad ^b R_w = \sum W^{1/2} \Delta F / \sum W^{1/2} F_o \quad (F > 2.0\sigma(F)).$$

Table 2. Relevant Bond Lengths and Angles for Cd(SOCC(CH₃)₃)₂TMEDA (1)

A–B	bond length (Å)	A–B	bond length (Å)
Cd(1)–S(1)	2.489(2)	Cd(1)–S(2)	2.480(2)
Cd(1)–N(1)	2.391(5)	Cd(1)–N(2)	2.394(5)
Cd(2)–S(3)	2.484(2)	Cd(2)–S(4)	2.493(2)
Cd(2)–N(3)	2.366(5)	Cd(2)–N(4)	2.371(5)
Cd(3)–S(5)	2.479(2)	Cd(3)–S(6)	2.485(2)
Cd(3)–N(5)	2.379(4)	Cd(3)–N(6)	2.357(5)

A–B–C	bond angle (deg)	A–B–C	bond angle (deg)
S(1)–Cd(1)–S(2)	133.7(1)	S(1)–Cd(1)–N(1)	112.2(1)
S(2)–Cd(1)–N(1)	103.7(1)	S(1)–Cd(1)–N(2)	104.6(1)
S(2)–Cd(1)–N(2)	111.2(1)	N(1)–Cd(1)–N(2)	77.3(2)
S(3)–Cd(2)–S(4)	131.8(1)	S(3)–Cd(2)–N(3)	110.7(1)
S(4)–Cd(2)–N(3)	107.6(1)	S(3)–Cd(2)–N(4)	108.3(1)
S(4)–Cd(2)–N(4)	107.5(1)	N(3)–Cd(2)–N(4)	77.8(2)
S(5)–Cd(3)–S(6)	130.0(1)	S(5)–Cd(3)–N(5)	112.5(1)
S(6)–Cd(3)–N(5)	108.4(1)	S(5)–Cd(3)–N(6)	108.2(1)
S(6)–Cd(3)–N(6)	107.8(1)	N(5)–Cd(3)–N(6)	77.4(2)

Table 3. Relevant Bond Lengths and Angles for Zn(SOCC(CH₃)₃)₂TMEDA (2)

A–B	bond length (Å)	A–B	bond length (Å)
Zn–N(1)	2.109(3)	Zn–N(2)	2.167(3)
Zn–S(2)	2.2910(11)	Zn–S(1)	2.3020(12)

A–B–C	bond angle (deg)	A–B–C	bond angle (deg)
N(1)–Zn–N(2)	85.96(13)	N(1)–Zn–S(2)	122.09(10)
N(2)–Zn–S(2)	111.86(9)	N(1)–Zn–S(1)	112.40(10)
N(2)–Zn–S(1)	104.67(10)	S(2)–Zn–S(1)	114.74(5)

SHELXL software was used for all computations (G. Sheldrick, Siemens XRD, Madison, WI).

Crystal Data for Zn(SOCC(CH₃)₃)₂TMEDA (2). ZnS₂·O₂C₁₆H₃₄N₂, Orthorhombic, *P*2₁2₁2₁, *a* = 10.0859(9) Å, *b* = 10.867(1) Å, *c* = 19.986(3) Å; *V* = 2190.6(4) Å³; *Z* = 4; *D*_c = 1.261 g/cm³; μ(Mo Kα) = 1.321 mm⁻¹; *T* = –40 °C, Siemens R3m/v, Mo Kα. Of 4521 data (2.04 ≤ 2θ ≤ 30), 4292 were independent and 2881 were observed [2σ(*F*_o)]. The structure was solved by direct methods. Refinement: all non-hydrogen atoms were refined anisotropically, all hydrogen atoms positions were allowed to vary, and the Flack parameter refined

to $-0.02(2)$, indicating that the correct absolute hand of the structure was determined. $R(F) = 4.33\%$, $R(WF) = 8.96\%$, $GOF = 0.978$, $N_O/N_V = 20.6$, $\Delta(r) = 0.672 \text{ e } \text{\AA}^{-3}$, $\Delta/\sigma(\text{max}) = 0.000$. SHELXL software was used for all computations (G. Sheldrick, Siemens XRD, Madison, WI).

Aerosol-Assisted Chemical Vapor Deposition (AACVD). The apparatus for AACVD and its operation has been described previously.^{7,14,18} Precursor solutions for $\text{Cd}_x\text{Zn}_{1-x}\text{S}$ were prepared by dissolving **1** and **2** in appropriate concentrations and ratios in toluene, and precursor solutions for ZnS:Mn were prepared by dissolving **2** and $\text{Mn}_2(\text{CO})_{10}$ (purchased from Aldrich, **3**) in appropriate concentrations and ratios. The air-stable precursors and precursor solutions were handled in the air.

Deposition of $\text{Cd}_x\text{Zn}_{1-x}\text{S}$. Experiments to determine the feed-rate-limited growth regime for deposition of $\text{Cd}_x\text{Zn}_{1-x}\text{S}$ were carried out with precursor solution stoichiometry (equal molar **1** and **2**), precursor solution concentration (10 mmol), volume of precursor solution (15 mL), carrier gas flow rate (2 Lpm), deposition time (25 min), preheating temperature (80 °C), and substrate size ($1 \times 1 \text{ cm}$) all kept constant, and substrate temperature was varied. Substrates were (100) silicon with $0.025 \mu\text{m}$ thermal oxide, SiO_2 layer. Film growth rates ($\text{\AA}/\text{min}$) were recorded by weighing the substrate prior to and after deposition, and film thicknesses were calculated from the mass of the deposited film. Once the feed-rate-limited growth regime was determined, the feed rate was changed by varying carrier gas flow rate or precursor solution concentration to observe the corresponding changes in film deposition rates. Finally, films of variable Cd:Zn ratio were deposited from precursor solutions of the same variable Cd:Zn ratio, using the deposition conditions which were determined to be feed-rate-limited.

Deposition of ZnS:Mn . The ZnS:Mn films were deposited from 10 mmol solutions of $\text{Zn}(\text{SOCC}(\text{CH}_3)_3)_2\text{TMEDA}$ with $\text{Mn}_2(\text{CO})_{10}$, with a preheating temperature of 80 °C, substrate temperatures of 250–300 °C, and a N_2 carrier gas tank regulator pressure of 35 PSI. Dopant levels of Mn ranged from ~ 1 –10 atomic percent. The ZnS:Mn films were deposited on substrates which were provided by Hewlett-Packard Labs, Fremont, CA; the substrates consisted of a glass/conductor ($0.12 \mu\text{m}$ indium tin oxide)/insulator ($0.30 \mu\text{m}$ SiO_{1-x}) stack which is used in display devices.

Characterization of Thin Films. The deposited films were analyzed by glancing angle X-ray diffraction to determine crystallinity, phase, and orientation; Auger electron spectroscopy (AES), electron microprobe, or secondary ionization mass spectroscopy (SIMS) to determine purity and stoichiometry of the films; and scanning electron microscopy (SEM) to examine the film morphologies. The glancing angle X-ray diffraction experiments were carried out on a Siemens D5000 operated at 35 kV with a $\text{Cu K}\alpha$ source (1.5406 \AA). Typical scan parameters for glancing angle experiments included 2° glancing angle, 20 – 90° detector angle, 0.04° step size and 5 s step time, and a 0.2 mm slit was used for a filter. Scanning electron microscopy (SEM) was carried out on a Hitachi S-800 instrument. Film samples were mounted both parallel and perpendicular to the electron beam to obtain plane and cross-sectional views.

Electron microprobe analyses were performed on a JEOL 733 electron microprobe at 10 kV accelerating voltage and 10 nA beam current with a Link/Oxford energy-dispersive spectroscopy (EDS) system. The films were carbon coated prior to analyses. Films were analyzed for Zn, Mn, S, C, and O. The ZAF ($Z = \text{atomic number}$, $A = \text{amplitude}$, $F = \text{frequency}$) matrix corrections were applied to the analyses, and EDS standard reference files were collected on sphalerite (Zn and S), Si metal (Si), carbon rod (C), spessartine garnet (Mn), and ZrO_2 (O) standards.

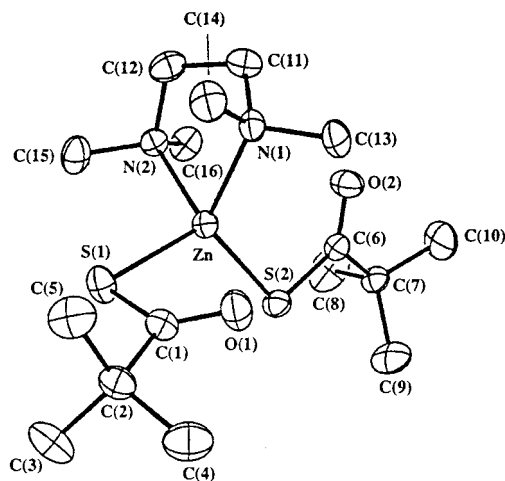


Figure 1. ORTEP plot of $\text{Zn}(\text{SOCC}(\text{CH}_3)_3)_2\text{TMEDA}$ (**2**) as determined by single-crystal X-ray diffraction.

Auger electron spectroscopy (AES) data were collected with a cylindrical mirror analyzer (PHI 10-155), with an electron beam energy of 3 keV, at a base pressure of 10^{-9} Torr. The Auger peaks of Zn (LMM) at 993 eV, Cd (MNN) at 375 eV, S (LMN) at 150 eV, C (KLL) at 271 eV, O (KLL) at 510 eV, and N (KLL) at 378 eV were used for estimation of the composition and stoichiometry of the $\text{Cd}_x\text{Zn}_{1-x}\text{S}$ films. Data were collected at a depth of 100–150 \AA below the film surface. Experimental sensitivity factors were obtained from Auger spectra of standard stoichiometric samples (powders and sputtered thin films) of the elements of interest, ZnS, ZnO, and CdS. At fixed sensitivity factors of oxygen and sulfur ($S_O = 0.5$; $S_S = 0.8$) from the experimental data for stoichiometric compounds, the following relative sensitivity factors were obtained and applied: $S_{\text{Zn}} = 0.53$ and $S_{\text{Cd}} = 0.53$ (for the above-mentioned Auger peaks). A secondary ion mass spectrometer (SIMS) was used to determine the Mn concentrations of the ZnS:Mn films for films with Mn concentrations less than or equal to 1 at. %. These measurements were conducted using a Cameca ims 4f instrument. For these measurements an isotopically filtered 160 primary beam was accelerated with a nominal 12.5 kV potential. The 100 nA beam was rastered over an area of approximately 200×200 microns. Secondary ions were collected from a $33 \mu\text{m}$ diameter region located at the center of the rastered region. The mass spectrometer was operated in peak-stepping mode which included five mass stations (^{30}Si , ^{32}S , ^{55}Mn , ^{64}Zn , and ^{66}Zn). Absolute Mn concentrations were calculated by comparing the observed $^{55}\text{Mn}/^{64}\text{Zn}$ ratios in the target to the same ratio as observed in a morphologically and compositionally similar sample which had a Mn content of 5.5 at. % (determined by electron microprobe).

Photoluminescence data for the ZnS:Mn were obtained at Hewlett-Packard Labs in Fremont, CA. For characterization of ZnS:Mn photoluminescence properties, an excitation spectrum and an emission spectrum were measured for each film using a xenon high-pressure lamp as an excitation source, and a cooled single-photon-counting system as a detection source. The excitation wavelength was changed by using a double monochromator. The excitation spectra were obtained by varying the excitation energy while observing the emission intensity at 590 nm, the maximum emission for the Mn center in a ZnS matrix. The emission spectra were collected by changing the observed wavelength of emission with a constant excitation energy of 340 nm (host lattice ZnS band gap energy) or 390 nm (Mn internal excitation bands).

Results and Discussion

The molecular structures of **1** and **2** are very similar, and the ORTEP of **2** is shown as an example in Figure 1. Both have distorted tetrahedral MS_2N_2 ($\text{M} = \text{Cd}, \text{Zn}$) coordination, with the monodentate thiopivalate ligands

(17) Beilstein 4-02-00-00917.

(18) Roger, C.; Corbitt, T.; Xu, C.; Zeng, D.; Powell, Q.; Chandler, C. D.; Nyman, M.; Hampdensmith, M. J.; Kostas, T. T. *Nanostruct. Mater.* **1994**, *4*, 529–535.

S-bonded to the metal and the oxygen double-bonded to the carbon. The cadmium derivative **2** has three unique molecules in the unit cell which differ slightly in bond lengths and angles, most likely the result of crystal packing. There are numerous other potential bonding modes of the thiocarboxylate ligand which include μ^2 -S, μ^2 -O,S,O chelation of a single metal center, bridging two metal centers (S-C-O bridge), or bonded to the metal through the oxygen with the sulfur double-bonded to the carbon. However, the bonding mode which is observed in **1** and **2** appears to be preferred by the ligand, as it is seen in the solid-state structures of a wide variety of molecular complexes which vary in identity of the metal, thiocarboxylate alkyl group (R) and additional supporting ligands.^{7,16,19-26} Fortunately, this preferred bonding mode appears to be the most suitable for formation of metal-sulfido materials by thiocarboxylic anhydride elimination.¹⁶

Growth Kinetics of Cd_xZn_{1-x}S Thin Films Deposited from **1 and **2**.** A series of experiments was carried out in order to determine the AACVD conditions over which the compositional control of Cd_xZn_{1-x}S deposited from a toluene solution containing a mixture of M(SOCC(CH₃)₃)₂TMEDA (M = Cd, Zn) is achievable. Additionally, the temperature ranges at which film growth rate are (1) under the control of some thermally activated process or (2) controlled by the precursor feed rate was investigated. The deposition rate (Å/min) was studied as a function of temperature (150–275 °C) where parameters which were held constant included precursor solution ratio (1:1 Zn(SOCC(CH₃)₃)₂TMEDA: Cd(SOCC(CH₃)₃)₂TMEDA) and concentration (10 mmol total), preheating zone temperature (80 °C), carrier gas flow rate (20 psi N₂, 2 L/min), deposition time (25 min), and approximate substrate size (1 cm × 1 cm). The results of these experiments are plotted as ln(deposition rate) vs 1/T in Figure 2. Over the temperature range of 150–165 °C, the deposition rate increased logarithmically with temperature, which suggests an activated process, probably either evaporation-rate-limited deposition (through evaporation of the precursor in the boundary layer above the substrate) or surface-reaction-rate-limited deposition. We speculate the activation energy in this temperature-dependent region of ~4 kcal/mol is more consistent with an evaporation-rate-limited regime (due to its relatively low value). Films deposited between ~180 and 225 °C exhibit relatively constant deposition rates, approaching 315 Å/min, consistent with feed-rate or transport-limited deposition.^{14,15}

The composition of all films from these experiments, except for that deposited at 275 °C, was Cd_{0.50}Zn_{0.50}S (±0.02) as determined by AES, where the error of AES

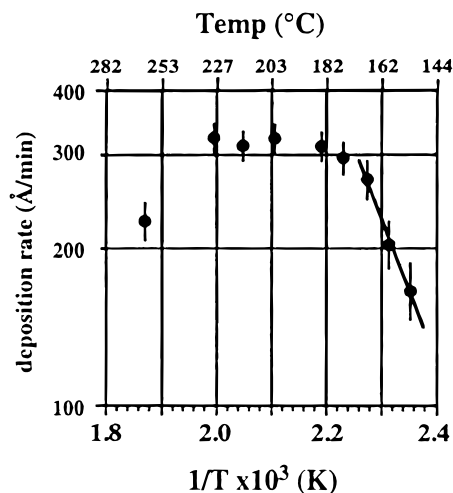


Figure 2. Plot of ln(deposition rate) vs 1/T (K) of films deposition from 1:1 Cd:Zn precursor solutions. The error bars are equal to ±12 Å/min. Three deposition regimes are observed: (1) deposition rate has an Arrhenius dependence on temperature from 150 to 170 °C; (2) temperature has minimal effect on deposition rate from 175 to 225 °C; (3) deposition rate decreases significantly above 250 °C, due to gas-phase reactions of the precursor.

is ±0.01. Additionally, the (002) peak position observed by X-ray diffraction corresponded with the Cd_{0.50}Zn_{0.50}S phase (2θ = 28.5°), and there was no evidence for other crystalline phases such as CdS or ZnS. The error in composition was mainly attributed to errors in weighing the precursors in the preparation of the solutions, since films deposited from the same stock precursor solution have similar deviations from the composition Cd_{0.5}-Zn_{0.5}S. The film deposited at 275 °C was analyzed to be Cd_{0.29}Zn_{0.71}S. This is likely a result of the gas-phase decomposition of the cadmium precursor which depletes the feed of cadmium precursor to the substrate, as was observed for CVD of CdS or Cd_xZn_{1-x}S from Cd(SOCC(CH₃)₃)₂TMEDA.⁷ However, the higher thermal stability of the pivalate analogue allowed for a window under which feed-rate-limited deposition and composition control was achievable, whereas no temperature window at which feed-rate-limited deposition of Cd_xZn_{1-x}S from the thioacetate precursors was observed under any of the experimental conditions examined.⁷ It was somewhat surprising that films deposited under evaporation-rate-limited conditions (150–170 °C) reflected the stoichiometry of the precursor solution, since we expect the zinc precursor to be more volatile, which under these conditions should result in a film with a higher zinc content than the precursor solution.

To confirm a precursor feed-rate-limited deposition regime between 180 and 225 °C, the precursor feed rate was increased by either increasing the N₂ carrier gas pressure (from 20 to 35 psi), thereby increasing the precursor feed rate, with a concomitant decrease in the time of deposition (from 25 to 15 min), or increasing the concentration of the precursor solution (from 10 to 20 mmol). All other experimental conditions were unchanged. The deposition rate at 200 °C was 620 Å/min with doubled precursor concentration and 585 Å/min with an increased carrier gas flow rate. Both films were Cd-deficient relative to the 1:1 Zn: Cd precursor solution, each with a composition of Cd_{0.35}Zn_{0.65}S. These results lend further evidence for feed-rate-limited deposition,

(19) Shang, G.; Kunze, K.; Hampden-Smith, M. J. *Adv. Mater. CVD*, **1996**, in press.

(20) Shang, G.; Hampden-Smith, M. J.; Duesler, E. N. *J. Chem. Soc., Chem. Commun.* **1996**, 15, 1733–1735.

(21) Shang, G.; Hampden-Smith, M. J.; Duesler, E. N. *Inorg. Chem.*, submitted.

(22) Bonamico, M.; Dessey, G.; Fares, V.; Scaramuzza, L. *J. Chem. Soc., Dalton Trans.* **1976**, 1, 67–70.

(23) Alsfasser, R.; Powell, A. K.; Trofimenko, S.; Vahrenkamp, H. *Chem. Ber.* **1993**, 126, 685–694.

(24) Denifl, P.; Bildstein, B. *J. Organomet. Chem.* **1993**, 453, 53–59.

(25) Okamoto, K.; Konno, T.; Hidaka, J. *Acta Crystallogr.* **1990**, C46, 216–218.

(26) Hall, M.; Sowerby, D. B.; Falshaw, C. P. *J. Organomet. Chem.* **1986**, 315, 321–328.

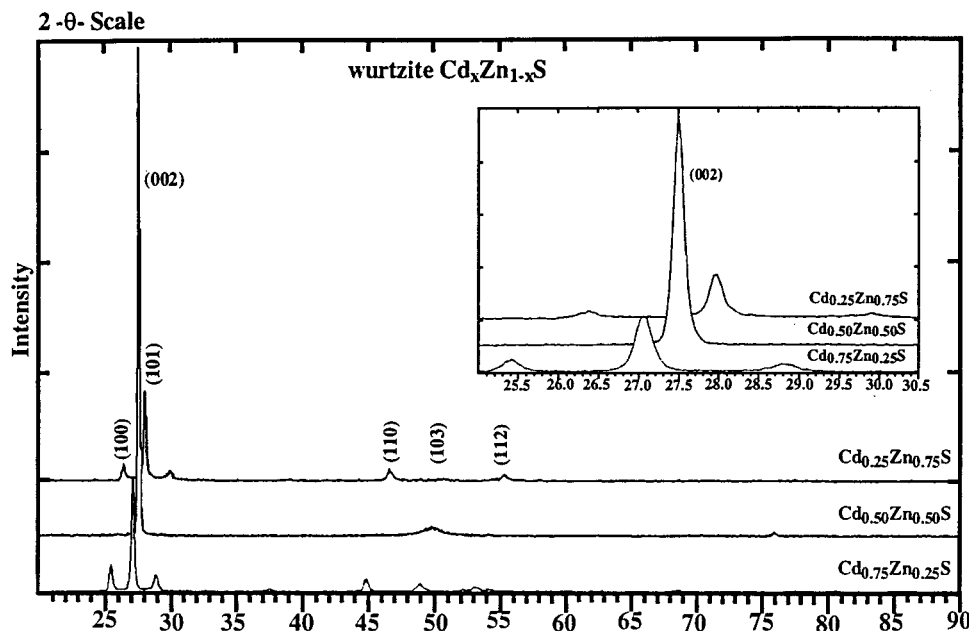


Figure 3. Glancing angle X-ray diffraction of films of composition $\text{Cd}_{0.25}\text{Zn}_{0.75}\text{S}$, $\text{Cd}_{0.50}\text{Zn}_{0.50}\text{S}$, and $\text{Cd}_{0.75}\text{Zn}_{0.25}\text{S}$ deposited at 225 °C. The films are hexagonal (wurtzite), distinguished from cubic (sphalerite) by the (100), (101), and (103) peaks. Inset: expanded (002) region of the spectra. A linear shift to larger 2θ is observed with increasing zinc. No binary ZnS (2θ (002) = 28.5°) or CdS (2θ (002) = 26.5°) is observed.

in that increasing the precursor feed rate by either increasing precursor concentration or increasing carrier gas flow rate results in an increased deposition rate. The deficiency of cadmium in the films relative to the precursor solution from which they were deposited suggests that more zinc precursor than cadmium precursor is reaching the substrate under these conditions of increased precursor feed rate. The cadmium precursor is probably depleted by incomplete evaporation relative to the zinc precursor due to lower volatility compared to the zinc analogue.²⁷

Characterization of $\text{Cd}_x\text{Zn}_{1-x}\text{S}$ Films. Glancing angle X-ray diffraction of $\sim 0.790 \mu\text{m}$ films (grown at $\sim 315 \text{ \AA}/\text{min}$) of compositions $\text{Cd}_{0.25}\text{Zn}_{0.75}\text{S}$, $\text{Cd}_{0.50}\text{Zn}_{0.50}\text{S}$, and $\text{Cd}_{0.75}\text{Zn}_{0.25}\text{S}$ deposited under "feed-rate-limited" conditions at 225 °C are shown in Figure 3. The films of the three compositions are the wurtzite polymorph and exhibit preferential growth on the (002) plane, where the $\text{Cd}_{0.5}\text{Zn}_{0.5}\text{S}$ film has the strongest preferential growth, and the $\text{Cd}_{0.75}\text{Zn}_{0.25}\text{S}$ film has the least preferential growth. This can be seen in the inset, which is the expanded region of the (002) peak. The (002) wurtzite peak of the $\text{Cd}_{0.50}\text{Zn}_{0.50}\text{S}$ phase is of greater intensity than that of $\text{Cd}_{0.25}\text{Zn}_{0.75}\text{S}$ and $\text{Cd}_{0.75}\text{Zn}_{0.25}\text{S}$ for films in equivalent thicknesses. Additionally, the $\text{Cd}_{0.25}\text{Zn}_{0.75}\text{S}$ and $\text{Cd}_{0.75}\text{Zn}_{0.25}\text{S}$ spectra also show the wurtzite (100) and (101) peaks in addition to the (002) peak which is indicative of more random growth. The (002) d spacing corresponding with the (002) peak agree with the (002) d spacings calculated by Vegard's law for solid solutions²⁸ for the three films, and Auger electron spectroscopy (AES) revealed that the films have the same stoichiometry as the precursor solutions from which they were deposited. Morphological differences

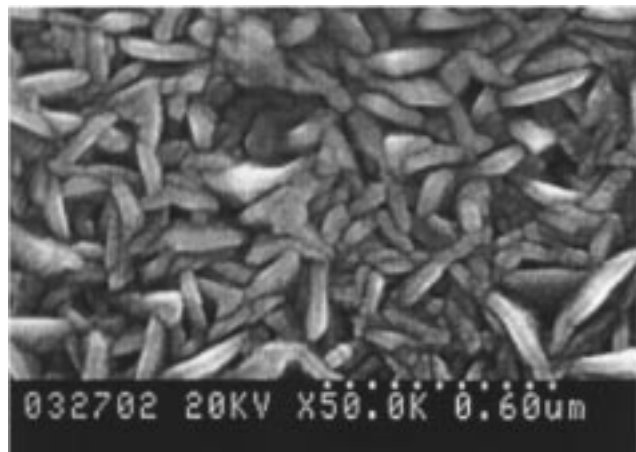
resulting from the different degrees of preferential growth on the (002) face can also be seen in the SEM images of the films in Figure 4. Films of compositions $\text{Cd}_{0.75}\text{Zn}_{0.25}\text{S}$, $\text{Cd}_{0.50}\text{Zn}_{0.50}\text{S}$, and $\text{Cd}_{0.75}\text{Zn}_{0.25}\text{S}$ which were deposited from thiopivalate precursor solutions of the same Cd:Zn ratio are shown in plane view. The $\text{Cd}_{0.75}\text{Zn}_{0.25}\text{S}$ film consists of more randomly oriented grains, whereas the films of composition $\text{Cd}_{0.50}\text{Zn}_{0.50}\text{S}$ and $\text{Cd}_{0.25}\text{Zn}_{0.75}\text{S}$ exhibit a columnar growth, which is most apparent in the $\text{Cd}_{0.50}\text{Zn}_{0.50}\text{S}$ film.

Deposition and Characterization of $\text{ZnS}:\text{Mn}$ Films. Using a feed-rate-limited deposition strategy (300 °C growth temperature, 10 mmol precursor solution, 2 Lpm carrier gas flow) $\text{ZnS}:\text{Mn}$ thin films were deposited from precursor solutions with Mn concentrations ranging from 1 to 8 at. %. A typical glancing angle X-ray diffraction spectrum of the ZnS host matrix with 1 at. % Mn deposited at 300 °C is shown in Figure 5. The crystalline phase is wurtzite with preferential growth on the (002) face. The Mn concentration was measured by electron microprobe for films of $\text{Mn} > 1$ atomic % and by SIMS for films of $\text{Mn} \leq 1$ at. %. Films were initially deposited with higher Mn concentrations in order to establish the ability to control the dopant levels, since quantification of film composition is more accurate at higher concentrations. The Mn concentrations of these films and of the precursor solutions from which they were deposited are summarized in Table 4. These results show that the concentration of manganese was similar to the concentration of the precursor solutions for ZnS films with 1–8 at. % manganese. Additionally SIMS analyses showed the Mn concentration to be uniform throughout the film depth, which suggests it is homogeneously dispersed in the ZnS host matrix.

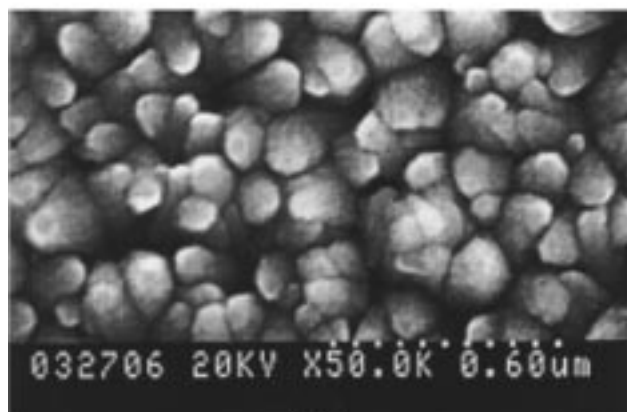
A typical photoluminescence emission and excitation spectrum of a $\sim 750 \text{ nm}$ thick $\text{ZnS}:\text{Mn}$ film (Mn concentration 1% by SIMS analysis) is shown in Figure 6. The excitation spectrum shows a maximum emission of 590

(27) Richardson, M. F.; Sievers, R. E. *Inorg. Chem.* **1971**, *10*, 498–504.

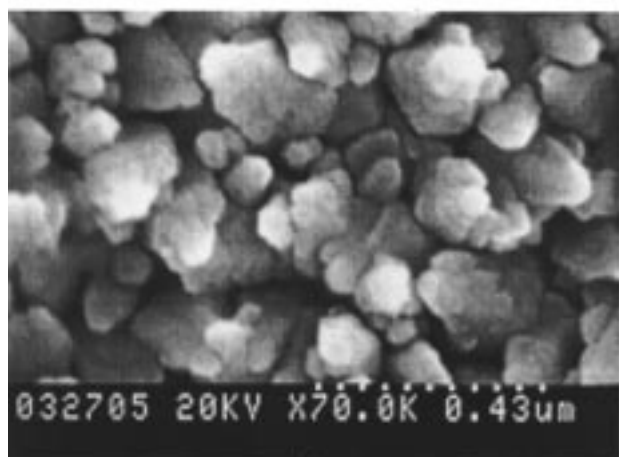
(28) West, A. R. *Solid State Chemistry and its Applications*; John Wiley & Sons: New York, 1984.



(a)



(b)



(c)

Figure 4. Scanning electron micrographs of $\text{Cd}_{0.75}\text{Zn}_{0.25}\text{S}$ (a), $\text{Cd}_{0.50}\text{Zn}_{0.50}\text{S}$ (b), and $\text{Cd}_{0.25}\text{Zn}_{0.75}\text{S}$ (c) deposited at 225 °C in plane view. The variations in film morphologies are also observed in the X-ray diffraction spectra, where the $\text{Cd}_{0.50}\text{Zn}_{0.50}\text{S}$ film shows the strongest preferred growth in the (002) direction, and the $\text{Cd}_{0.75}\text{Zn}_{0.25}\text{S}$ (a) film shows the least preferred growth.

nm (yellow) when the excitation source is 335 nm (ZnS band gap). Conversely, with an excitation energy of 335 nm, emission maxima of 590 nm (yellow) and 700 nm (red) are observed, which are the main luminescent wavelengths of ZnS:Mn. Emission spectra obtained with excitation energies of 380 and 467 nm gave

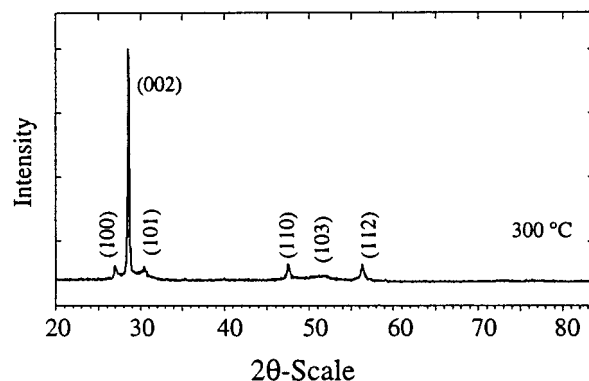


Figure 5. Glancing angle X-ray diffraction spectrum of wurtzite phase ZnS:Mn deposited at 300 °C.

Table 4. Mn Concentration for Precursor Solutions and Corresponding ZnS:Mn Thin Films

film number	Mn concn of precursor solution (mol %)	Mn concn of film (at. %)
1 ^a	5.0	5.5
2 ^a	4.0	3.7
3 ^a	3.0	3.2
4 ^a	2.0	2.3
5 ^b	1.0	0.9

^a Measured by electron microprobe (error = ±1). ^b Measured by SIMS (error = ±0.1).

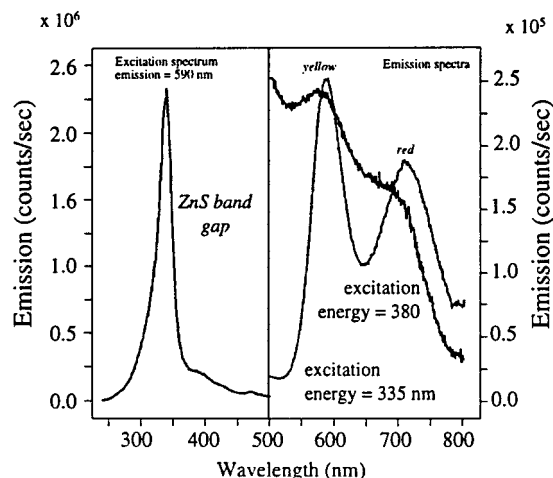


Figure 6. Excitation (left) and emission (right) photoluminescence spectra of ZnS:Mn thin films.

emission maxima characteristic of internal excitation bands of Mn.

Although the luminescence spectra of the films deposited by AACVD show characteristics typical of ZnS:Mn, the brightness was relatively weak.²⁹ The weak luminescence might be attributed to surface roughness⁹ created by the columnar morphology of the ZnS host matrix, such as that observed in the micrograph in Figure 7. The surface roughness of the ZnS:Mn films might be improved by depositing the films under conditions which favor more random growth rather than preferred growth on the (002) face. Deposition conditions which favor more random growth include (1) increased deposition temperature, (2) increased carrier gas flow rate, or (3) increased precursor solution concentration. However, as described previously, increase

(29) Personal communication with Dr. Regine Mueller-Mach, H. P. L., Palo Alto, CA.

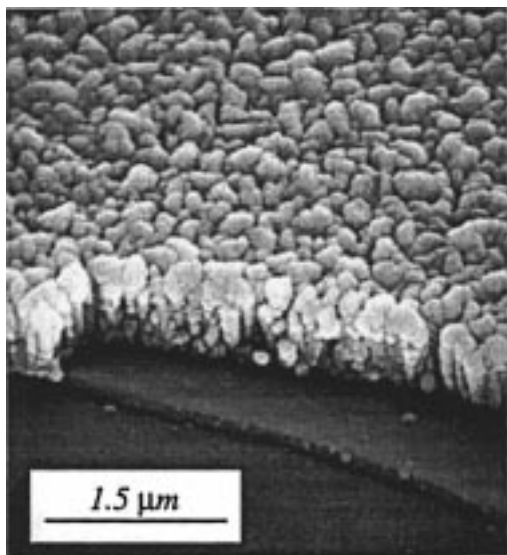


Figure 7. Micrograph of ~ 750 nm ZnS:Mn deposited at 300 °C. The SiON_{1-x} insulator layer is seen directly below the ZnS:Mn film, and the indium tin oxide (ITO) conductor layer is beneath the SiON_{1-x} layer.

in carrier gas flow rate or increase in precursor solution concentration might result in loss of the feed-rate-limited growth and thus loss of compositional control. Varying deposition conditions and also exploring the use of alternative precursors to obtain films with improved luminescence behavior resulting from smoother surface morphology, while maintaining control over dopant levels, is the focus of continued work.

Conclusions

In summary, this work has shown that thin-film ternary materials such as $\text{Cd}_x\text{Zn}_{1-x}\text{S}$ and ZnS:Mn can be synthesized from mixtures of precursors with control over the composition by using (1) precursors with matched reactivity, (2) aerosol-assisted delivery of precursor solutions (AACVD), and (3) feed-rate-limited deposition conditions. Deposition of $\text{Cd}_x\text{Zn}_{1-x}\text{S}$ with

control over x was accomplished at 225 °C under feed-rate-limited conditions from the new thiopivalate precursors, $\text{M}(\text{SOCC}(\text{CH}_3)_3)_2\text{TMEDA}$ ($\text{M} = \text{Cd}, \text{Zn}$). Films were impurity-free and well-crystallized, and this work provides the first example of CVD of $\text{Cd}_x\text{Zn}_{1-x}\text{S}$ with compositional control. Also by using AACVD and the feed-rate-limited strategy, ZnS:Mn was deposited from $\text{Mn}_2(\text{CO})_{10}$ and $\text{Zn}(\text{SOCC}(\text{CH}_3)_3)_2\text{TMEDA}$ at 300 °C with control over composition for Mn dopant levels of 1–8%. The SIMS analyses showed the Mn concentration to be uniformly dispersed throughout the ZnS film, and photoluminescence analyses of 1 at. % Mn doped films showed typical excitation and emission energies of ZnS:Mn. Work toward improving luminescence behavior through modification of film morphology while maintaining compositional control is ongoing.

The understanding of CVD deposition strategies to control film composition is crucial to emerging phosphor displays technologies. We are continuing to apply AACVD and feed-rate-limited strategies to the synthesis of other doped phosphor materials such as $\text{CaGa}_2\text{S}_4:\text{Ce}$ and $\text{Cd}_x\text{Zn}_{1-x}\text{S}:\text{Ag}$.

Acknowledgment. We thank the Office of Naval Research for financial support of this work, Dr. Paolina Atanassova for AES measurements, Dr. Michael Wiedenbeck (UNM Dept of Earth and Planetary Sciences) for SIMS analyses, Mike Spilde (UNM Dept of Earth and Planetary Sciences) for electron microprobe analyses, Dr. Regina Mueller-Mach (Hewlett-Packard Labs, Palo Alto, CA) for the photoluminescence measurements and also providing the substrates, the Camille and Henry Dreyfus Foundation for purchase of the X-ray diffractometer, and Nena Davis for technical assistance.

Supporting Information Available: Tables of crystal data, positional and thermal parameters, and a full listing of bond distances and angles for **1** and **2** (29 pages); tables of structure factors (37 pages). Ordering information is given on any current masthead page.

CM9706816